JOURNAL OF CATALYSIS 157, 321–333 (1995)

Sol-Gel Synthesis of Zirconia Supports: Important Properties for Generating *n*-Butane Isomerization Activity upon Sulfate Promotion

David A. Ward[1] and Edmond I. Ko[2]

Department of Chemical Engineering, Carnegie Mellon University, Pittsburgh, Pennsylvania 15213-3890

Received May 5, 1995; revised July 20, 1995; accepted July 21, 1995

By studying zirconium oxide supports prepared by a variety of methods, we determined the characteristics required of a zirconia support for the generation of *n*-butane isomerization activity after sulfate impregnation. Using sol-gel chemistry and supercritical drying, we formed a zirconia aerogel and examined two different sulfate promotion points: (i) after drying the aerogel at 383 K and (ii) after calcination at 773 K. All sulfated aerogels, given the appropriate activation temperature, were active for *n*-butane isomerization, but had very different textural properties and activation behaviors depending on the sulfate introduction point. In addition, as the aerogel support after 773 K heat treatment was crystalline tetragonal, we demonstrated that crystalline zirconia can be impregnated with sulfate to give an active sample, in contrast to previous literature results. From a comparison of this calcined aerogel with other calcined supports prepared from preformed zirconia sols or commercially available zirconia, the hydroxyl content of the surface was shown to be the determining factor in whether a support could form an active sample from sulfate promotion. The sol-gel preparation of zirconia yielded materials with a high hydroxyl content, even after calcination, which allowed for successful sulfate impregnation.

INTRODUCTION

Sulfate-promoted zirconium oxide (zirconia, ZrO_2) has been widely studied in recent years (1–4), due particularly to its potential catalytic application in the petrochemical industry for alkane isomerization and other hydrocarbon reactions. Often considered a solid superacid, sulfated zirconia derives its catalytic properties from a very strong surface acidity that gives the material a high activity at low temperatures.

The majority of work done on sulfated zirconia uses a preparation method similar to the first method reported (5): A zirconium hydroxide is formed by a solution-precipitation method typically starting with a dissolved zirconium salt or alkoxide as a precursor and causing precipitation with ammonium hydroxide. This hydrous zirconia is dried at low temperatures (<423 K) and then promoted with sulfate ions using sulfuric acid or ammonium sulfate. The sulfated hydroxide is then dried and calcined to appropriate activation temperatures (773–923 K). While many variations of this synthesis have been performed, such as varying the zirconium precursor or pH of precipitation, most syntheses follow the procedure of placing a sulfate ion on a hydrous zirconia.

The role of the zirconia support is not fully understood in the sulfating mechanism. Some of this uncertainty is due to the fact that until now only the hydroxide of zirconia could be impregnated to form a material that exhibits catalytic activity. When zirconia is synthesized by the solution-precipitation method described above, it crystallizes upon calcination at temperatures above ca. 673 K. When sulfate is impregnated on this calcined, crystalline zirconia, the sulfated material is not catalytically active for reactions requiring a strong acid catalyst. The conclusion drawn was that superacidity cannot be generated by impregnating sulfate on a crystalline support and that the amorphous hydroxide must be used (3, 5–8). There is one lone report of a calcined zirconia being active for *n*-butane isomerization after sulfate impregnation (9) although no explanation for this observation was given.

To demonstrate the importance of the zirconia support in determining acidic properties, we have examined different points and methods of sulfate introduction in addition to putting sulfate on the zirconium hydroxide. Using the sol-gel method, we have developed previously a one-step synthesis of zirconia–sulfate aerogels (10). In this preparation, zirconia support formation and sulfate promotion were combined by including sulfate ions during the zirconia gelation step. After supercritical drying, a mixed zirconia–sulfate aerogel was formed. This material had unusual activation behavior given that sulfate was included in the bulk of the aerogel, rather than on the surface as is the case for an impregnated sample. It was this activation behavior that allowed us to reach conclusions about the type of acidity

[1] Current address: Shell Chemical Co., Westhollow Technology Center, P.O. Box 1380, Houston, TX 77251-1380.

[2] To whom correspondence should be addressed.

0021-9517/95 $12.00

and sulfate species required on the surface of sulfated zirconia for *n*-butane isomerization activity to be seen.

In the present work, we used the flexibility of the sol-gel method to study another point of sulfate introduction. A sulfated zirconia that was active for *n*-butane isomerization was formed by impregnating a calcined, crystalline zirconia aerogel. By comparing calcined zirconia supports that formed catalytically active materials with supports that did not, we were able to determine the important properties required of a zirconia support to form an active sample upon sulfate impregnation.

EXPERIMENTAL

Sample Preparation

Zirconia aerogels were prepared following the standard procedure given in detail elsewhere (11) and summarized here. To form an alcogel, 16.2 ml of zirconium *n*-propoxide (70 wt% in propanol, Alfa) was diluted in a mixture of 15 ml of *n*-propanol (Fisher) and 1.90 ml of HNO_3 (70% w/w, Fisher). In a second beaker, 1.31 ml of distilled water (2.0 mol H_2O/mol Zr^{4+}) was mixed with another 15 ml of *n*-propanol. The water/alcohol mixture was added to the alkoxide/acid/alcohol mixture and stirred with a magnetic stir bar until gelation caused the vortex created by the stirring to disappear. The elapsed time between mixing and the disappearance of the vortex was recorded and called the gel time. All gels made in this study had identical gel times of 21 s.

The alcogel was covered with Parafilm and aged for 2 h at room temperature. The alcohol was then removed by supercritical drying with carbon dioxide (12). In a supercritical extraction screening system (Autoclave Engineers, Model 08U-06-60FS), supercritical CO_2 was flowed through the gel at ca. 343 K and 20.7×10^3–24.7×10^3 kPa with a downstream flow rate of 85 liters/h at ambient conditions. The supercritical drying process continued until no condensed alcohol could be collected downstream of the extraction vessel, indicating a complete displacement of the alcohol solvent by CO_2. A typical run lasted approximately 2 h. After removal of the CO_2, the resultant powder, an aerogel, was ground into a powder of <100 mesh.

The first heat treatment step consisted of drying the powder at 383 K for 3 h under a vacuum of 3.4 kPa. When desired, calcination was performed under flowing oxygen (24 liters/h) in a quartz tube inside a tubular furnace. The sample was heated at a rate of 10 K/min to the desired temperature and held at that temperature for 2 h. Samples calcined to 973 and 1173 K were previously calcined to 773 K. Aerogel supports are designated as A-ZrO_2.

The zirconia was promoted with sulfate in three different ways. A zirconia–sulfate co-gel was formed by including sulfate ions during the gelation step (10). Sulfuric acid (95–98%, Certified ACS, Fisher), which was used as the sulfate source, was added to the alkoxide/acid/alcohol mixture with a corresponding reduction in nitric acid to maintain a constant acid volume of 1.90 ml. These co-aerogels are designated as A-ZSO_4 XX, where XX is the nominal mole percentage zirconia in the sample (e.g., A-ZSO_4 90 is a zirconia–sulfate aerogel with 10 mol% sulfate). A second sulfate introduction method used the incipient wetness impregnation of ammonium sulfate onto the zirconia aerogel after the first 383 K drying step. The appropriate amount of ammonium sulfate (Alfa, ultrapure) to give a nominal 10 mol% sulfate loading was dissolved in a predetermined amount of distilled water whose volume would fill the pores of the aerogel to just below incipient wetness. This solution was then added dropwise with stirring to the dry powder. The impregnated powder was then dried under vacuum at 383 K for 3 h and subsequently calcined as desired. This sample is designated as A-Z-383/SO_4. The third sulfate introduction route was similar to the A-Z-383/SO_4 method except that the zirconia support used was an aerogel calcined at 773 K. This sample is designated as A-Z/SO_4. In the text and figure captions, "activation temperature" refers to the calcination temperature used for heating a sulfated sample and, as such, can be viewed as the heat treatment used to generate an active sulfate species.

Zirconia was also made from a preformed sol rather than an alkoxide (13). Zirconia sols, provided by Nyacol Products Inc., of 5–10 and 100 nm in size were used (Nyacol designations Zr10/20 and Zr100/20, respectively). Sols were gelled by the addition of ammonium hydroxide (28%, ACS Reagent, Fisher) in a ratio of 0.3 mol NH_4OH to mol HNO_3 found in the sol mixture. The required amount of NH_4OH was added to a volume of water that when mixed with 15 ml of the precursor sol would form a 0.714 *M* solution of ZrO_2. Mixing the ammonium hydroxide solution with the precursor, followed by vigorous stirring, formed a gel. After aging for 2–3 h, the gel was dried for 3 h at 383 K under a vacuum of 3.4 kPa. The dried samples were covered, allowed to sit overnight, and finally ground to <100 mesh and calcined at 773 K. These sol-derived samples are designated YY ZrO_2, where YY is the starting sol size in nanometers. Sulfate incipient wetness impregnation was then performed in the same manner as described above. The sulfated samples are designated as YY Zr/SO_4.

The preformed sols were also used to make zirconia–sulfate co-gels by adding ammonium sulfate to the sols before gelation. Sulfuric acid was not used as a sulfate source because its addition to the sol caused precipitation. For the 10 nm sol, the amount of ammonium sulfate required to give 10 mol% sulfate was dissolved in water and added to the preformed sol. The subsequent addition of ammonium hydroxide caused gelation. All preparative parameters, besides the sulfate content, were kept the same as the pure zirconia sol synthesis. In the case of the 100 nm sol, addition of ammonium sulfate caused gelation before

TABLE 1

Zirconia Support and Sulfated Zirconia Characteristics

Support[a]	BET (m^2/g)	Pore volume (cm^3/g)	Crystal phase[b]	Sulfated sample[c]	BET (m^2/g)	Crystal phase	*n*-Butane isom. rate (10 min/90 min) ($\mu mol/m^2/h$)
A-ZrO_2 383 K	231	0.658	A	A-Z-383/SO_4	25	T	7.49/4.59
A-ZrO_2	122	0.352	T	A-Z/SO_4	108	T	4.05/1.11
MEI $Zr(OH)_4$	120	0.133	T/trace M	M-$Zr(OH)_4$/SO_4	89	T/39% M	3.01/0.58
MEI $Zr(OH)_4$ 973 K	48	0.100	M/34% T	M-$Zr(OH)_4$-973/SO_4	42	M/31% T	Inactive
MEI ZrO_2	25	0.162	M	M-ZrO_2/SO_4	25	M	Inactive
Degussa ZrO_2	45	0.672	M/45% T	D-ZrO_2/SO_4	45	M/24% T	Inactive
10 ZrO_2 (10 nm sol)	30	0.0264	T	10 Zr/SO_4	24	T	Inactive
100 ZrO_2 (100 nm sol)	156	0.174	Weak M/trace T	100 Zr/SO_4	130	Weak M	0.37/trace
10 Zr sol as received				10 $ZrSO_4$	67	T/trace M	Inactive
100 Zr sol as received				100 $ZrSO_4$	122	Weak M	0.51/trace

[a] Supports calcined for 2 h at 773 K unless another temperature is indicated.
[b] Determined by X-ray diffraction: A, amorphous; T, Tetragonal; M, Monoclinic. Dominant phase listed first followed by vol% of minor phase.
[c] Sulfated samples calcined at 873 K for 2 h.

ammonium hydroxide addition. Thus, no ammonium hydroxide was required. The differences in the synthetic protocol for making the 10 and 100 nm zirconia sol–sulfate co-gels do not impact our results because our previous work (13) showed that the starting sol size is the only parameter that significantly affects the properties of the zirconia derived from preformed sols. Once a co-gel was made, it was treated exactly as an undoped sol-derived zirconia. These samples are designated YY $ZrSO_4$, where YY is the starting sol size in nanometers.

Finally, commercial zirconia samples were also examined. Zirconium oxide (E101) and zirconium hydroxide (XZO 631/01) were provided by MEI and zirconium oxide was provided by Degussa. Samples were vacuum dried and calcined at 773 K as described above. Note that the MEI $Zr(OH)_4$ may no longer be a hydroxide after calcination. However, it will still be referred to as $Zr(OH)_4$ as an indication of its origin. Sulfate impregnation was done by the incipient wetness impregnation of ammonium sulfate as described above to yield a nominal 10 mol% sulfate loading. Sample designations are M-ZrO_2/SO_4, M-$Zr(OH)_4$/SO_4, and D-ZrO_2/SO_4, respectively. Table 1 summarizes the notations of all the samples in this study, both for the supports and their sulfated counterparts.

Sample Characterization

Textural characterization was performed on an Autosorb-1 gas sorption system (Quantachrome Corp.). Samples were first outgassed for 3 h under vacuum at 473 K. Forty-point adsorption and desorption isotherms were obtained, from which BET surface area (taken at $P/P_0 \sim 0.3$), total pore volume (P/P_0 close to unity), microporosity (*t*-method), and pore size distribution (BJH method) were calculated. Crystal structure determinations were made by X-ray diffraction (XRD) using a Rigaku D/Max Diffractometer with CuKα radiation. The volume fractions of the tetragonal and monoclinic phases of zirconia were determined from the XRD patterns using the method of Toraya *et al.* (14). Thermogravimetry was done on a Cahn 113 thermogravimetry microbalance with the weight being electronically processed by a Cahn 2000 recording electrobalance. A Mattson Galaxy 5020 FTIR with a Harrick diffuse reflection attachment (DRA-2) was used to collect diffuse reflectance infrared (DRIFT) spectra. Spectra were taken using a DTGS detector over a range of 400–4000 cm^{-1} with a resolution of 2 cm^{-1}. Samples were powder diluted in KBr. *In situ* DRIFT experiments were performed in a Harrick reaction chamber (HVC-DR2).

Isomerization of *n*-butane was performed in a differential, downward flow, fixed-bed catalytic reactor. Approximately 500 mg of catalyst was pretreated under He flow (3 liters/h, Matheson HP) at 588 K for 1 h. The sample was then cooled to 553 K and exposed to the feed stream mixture of hydrogen (1.79 liters/h, Matheson UHP) and *n*-butane (0.079 liters/h, Matheson CP). A Gow-Mac 550P gas chromatograph with thermal conductivity detector (Column: Supelco 23% SP1700 on 80/20 Chromosorb, $\frac{1}{8}$ in. × 13 ft) was used to determine the composition of the product stream. Isomerization rates are reported on a per-surface-area basis.

RESULTS

Physical Characterization of Supports

Table 1 summarizes the support characteristics. The aerogel after drying at 383 K had a high surface area and pore

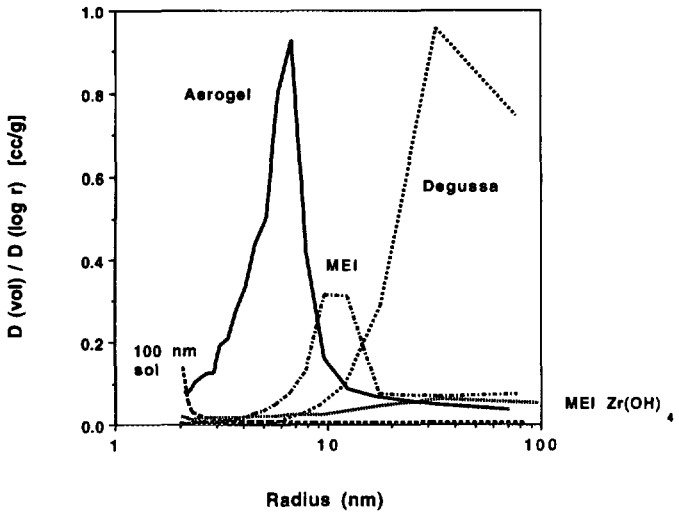

FIG. 1. Pore size distribution of zirconia supports after calcination at 773 K for 2 h. Not shown is the 10-nm sol sample, which is similar to the 100-nm sol sample.

volume and was X-ray amorphous. Upon calcination at 773 K, the surface area decreased to 122 m^2/g and the powder crystallized into the tetragonal phase. The MEI zirconium hydroxide had characteristics similar to those of the aerogel after 773 K calcination, except for its pore volume which was about one-third of that for the aerogel. Between the MEI zirconium hydroxide and MEI zirconia samples, the major differences were a lower surface area and a monoclinic structure for MEI ZrO_2. The Degussa sample also had a low surface area, but a high pore volume. It was a mixture of the tetragonal and monoclinic phases. The sol-derived zirconia samples had very different characteristics depending on the starting sol size. While the 10 nm sol support was crystalline tetragonal, the 100-nm sample was only weakly crystalline and primarily in the monoclinic phase with some trace of tetragonal structure. However, both samples were microporous, contrasted to all of the above samples which were primarily mesoporous. Pore size distributions for these samples are shown in Fig. 1.

Physical Characterization of Sulfated Materials

Sulfate was impregnated on the surface of these supports by incipient wetness impregnation with ammonium sulfate. Table 1 shows some of the properties of these sulfated materials next to the properties of the supports. It should be noted that the surface areas reported for the sulfated materials were after 873 K calcination while the support surface areas were after 773 K calcination. Thus, small decreases in specific surface area were due to sintering and the increased sample weight due to the sulfate. When the dried aerogel was impregnated and then calcined, we saw a significant drop in surface area. This was in contrast to literature reports in which sulfate impregnation of a hydroxide retarded sintering and yielded a higher surface area than undoped zirconia after calcination. The zirconia aerogel that was sulfate impregnated after calcination did not undergo this large decrease in surface area. In general, the crystal structure did not change with sulfate impregnation, except for a small amount of tetragonal-to-monoclinic transformation due to the increased calcination temperature. The exception is the amorphous aerogel dried at 383 K, which after impregnation crystallized into the tetragonal phase upon calcination.

Effect of Introduction Point on Sulfated Aerogels

We investigated the effect of the point of sulfate introduction on the activation and properties of the sulfated aerogel samples. This was done to complement our previous work on zirconia–sulfate co-gels (10), which showed that changes in the preparation, specifically sulfate content, changed the activation profile of the material. Figure 2 shows the changes in surface area with increasing activation temperature for the different sulfate introduction points. For A-Z-383/SO_4, the surface area gradually increased with increasing activation temperature with a corresponding increase in microporosity. The A-Z/SO_4 sample maintained a relatively constant surface area with activation temperature. The co-gel sample (10) decreased in surface area. These last two samples, as well as pure zirconia, exhibited no microporosity. Thus, we saw three very different behaviors with the three different sulfate introduction points.

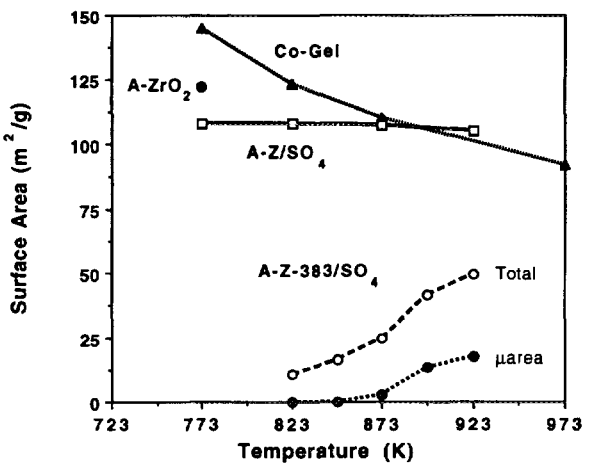

FIG. 2. Effect of activation temperature on the surface area of sulfated zirconia aerogels. Samples were calcined at the indicated temperature for 2 h. For A-Z-383/SO_4, both the total BET surface area and the micropore surface area, as determined from the *t*-plot, are shown. The surface area of the unsulfated zirconia aerogel support (A-ZrO_2) is given as a reference.

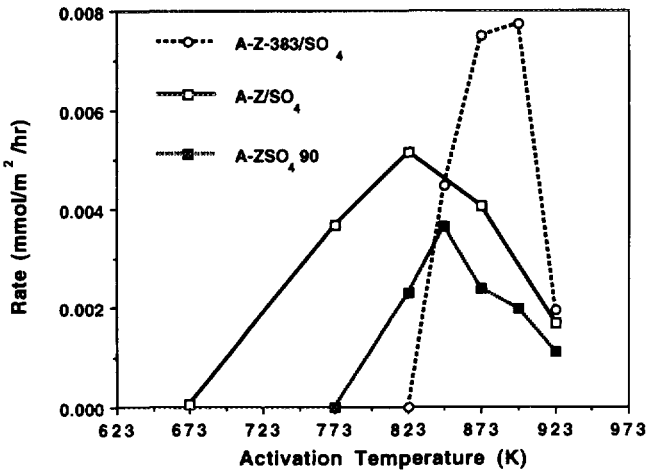

FIG. 3. Effect of activation temperature on the rate of *n*-butane isomerization over sulfated zirconia aerogels. Samples were calcined at the indicated temperature for 2 h. Data were taken after 10 min time on stream.

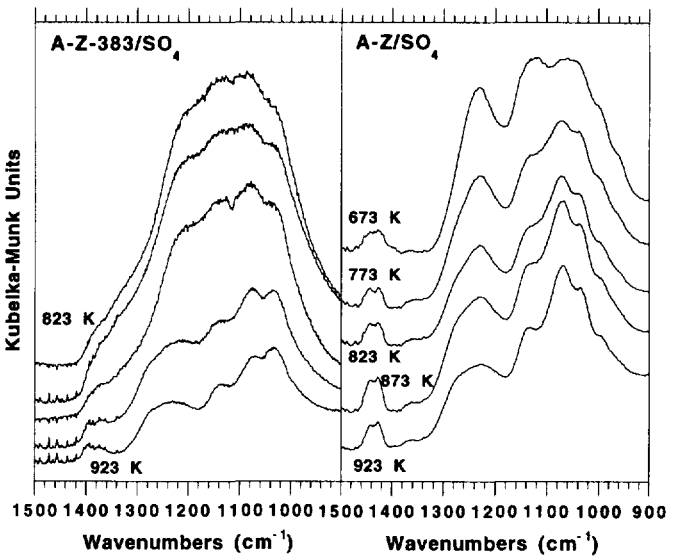

FIG. 5. Diffuse reflectance infrared spectra of sulfate-impregnated zirconia aerogels. Samples were calcined at the indicated temperature for 2 h. Left: Spectra were taken at 25 K intervals between 823 K (the top spectrum) and 923 K (the bottom spectrum). Spectra were taken under ambient conditions.

Figure 3 shows the effect of activation temperature on the rate of *n*-butane isomerization, reported on a per-surface-area basis, over the sulfated aerogels. We found different activation behavior for each sulfate introduction point. The A-Z-383/SO_4 sample showed the narrowest activation window as well as the highest specific reaction rate. The 10 mol% co-gel (10) exhibited a broader window but a smaller reaction rate. Finally, the A-Z/SO_4 sample showed the broadest range of activation temperatures that formed active samples.

Figure 4 shows the differential TG weight loss due to sulfate decomposition during a 10 K/min heat ramp. For the co-gel samples, we saw two types of weight loss (10). A low temperature mode (Mode I), evidenced by a narrow peak centered between 873 and 1000 K, corresponded to sulfate lost during expulsion from the bulk during crystallization. The second weight loss mode (Mode II) was due to sulfate decomposition from the surface and occurred over a broader temperature range above 1000 K. In Fig. 4, we see that A-Z-383/SO_4 demonstrated a Mode I-type peak centered around 1030 K followed by a small, broad Mode II peak. A-Z/SO_4 showed only Mode II weight loss.

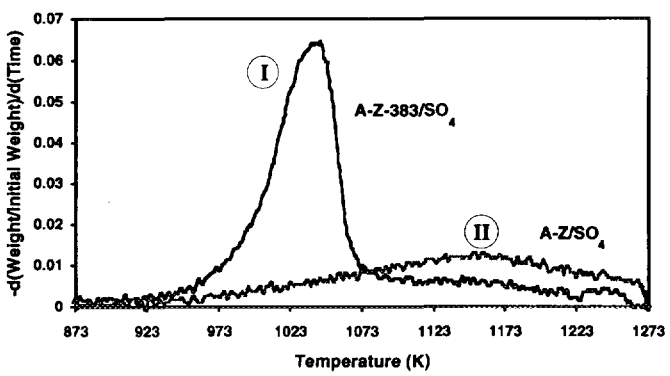

FIG. 4. Thermogravimetry scans of sulfate-impregnated zirconia aerogels. Samples were calcined at 873 K for 2 h.

Differences between the two sulfate impregnation points can also be seen in the DRIFT spectra of the sulfate region for the two impregnated aerogels (Fig. 5). The left panel of Fig. 5 shows the DRIFT spectra of A-Z-383/SO_4 after activation temperatures of 823 to 923 K. We see that the sulfate region changed shape with increasing activation temperature. At low activation temperatures, a broad superposition of peaks existed, which upon heat treatment separated into distinct peaks at 1036, 1076, 1136, and 1220–1270 cm^{-1}. This behavior and the peak locations at higher activation temperatures were the same as those seen for the co-gel samples (10). For the A-Z/SO_4 sample, we saw only very small changes in the sulfate region with increasing activation temperature. Peaks were observed at 1000, 1038, 1072, 1138, and 1230–1270 cm^{-1}. The 1270 and 1072 cm^{-1} peaks grew with increasing activation temperature. The features above 1350 cm^{-1} were due to the zirconia support and varied depending on preparation method.

Important to note was our ability to impregnate a calcined, crystalline support (A-ZrO_2 773 K) to produce an active sample (A-Z/SO_4) for *n*-butane isomerization. As mentioned above, most previous studies claimed that a calcined, crystalline material, when impregnated with

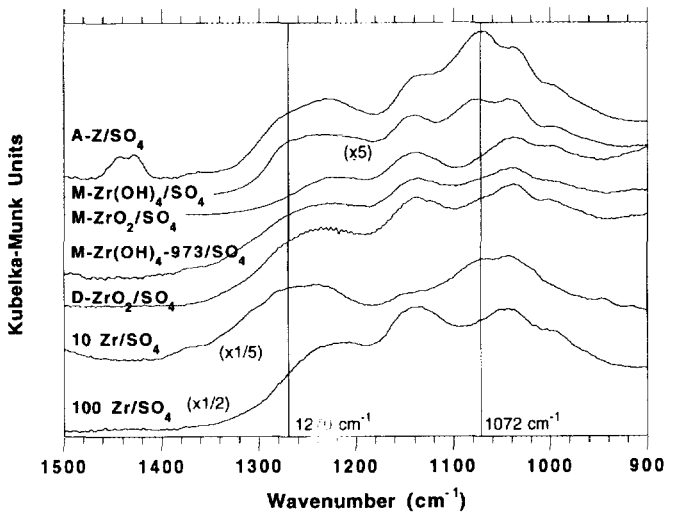

FIG. 6. Diffuse reflectance infrared spectra of sulfate-promoted zirconias. Samples were calcined at 873 K for 2 h. Spectra were taken under ambient conditions.

sulfate, was inactive for this reaction. Only one study found otherwise (9). This issue is addressed in detail below.

Impregnation of Other Zirconia Supports

n-Butane isomerization. To address why our zirconia aerogel preparation was able to form an active catalyst for isomerization by impregnating a calcined material when other preparation methods could not, we examined other calcined zirconia supports. We compared the characteristics of the supports with their ability to form active samples upon sulfate impregnation. All of the supports were calcined at 773 K for 2 h. Then, sulfate was introduced by the incipient wetness impregnation of ammonium sulfate. After drying in vacuum, the impregnated samples were then activated at 873 K and tested for their activity in *n*-butane isomerization. The activation temperature of 873 K was chosen because all samples capable of forming isomerization activity were typically active after this activation step (see Fig. 3). The last column in Table 1 shows the isomerization results. In addition to the calcined aerogel, the calcined MEI zirconium hydroxide also was active after impregnation and showed roughly similar activity to that of the aerogel. Zirconia formed from the 100 nm preformed sol also showed some activity when used as a support, although it was an order of magnitude less active. All of the other supports were inactive.[3] To test the effect of a more severe support preteatment, we calcined the MEI zirconium hydroxide to 973 K and then impregnated it. This impregnated sample (M-$Zr(OH)_4$-973/SO_4) was inactive. The sol–sulfate co-gels exhibited isomerization activity similar to that of the impregnated calcined sols.

Sulfate DRIFT spectra of sulfated zirconia. We could also see differences among these samples by looking at the sulfate region of *ex situ* DRIFT spectra. Figure 6 shows the DRIFT spectra of sulfated samples after 873 K activation. All of the samples have the common peaks located at ca. 1000, 1040, 1140, and 1220–1240 cm^{-1}. Some samples exhibited two additional peaks: one at ca. 1072 cm^{-1} and a shoulder at ca. 1270 cm^{-1}. These additional peaks were most clearly seen on A-Z/SO_4, M-$Zr(OH)_4/SO_4$, and 10 Zr/SO_4, all of which contained primarily tetragonal zirconia. M-$Zr(OH)_4$-$973/SO_4$ and D-ZrO_2/SO_4 both showed traces of these two peaks and contained a mixture of tetragonal and monoclinic zirconia. Sulfated samples (M-ZrO_2/SO_4 and 100 Zr/SO_4) that did not show these two peaks contained only monoclinic zirconia. So, the peaks at 1072 and 1270 cm^{-1} were due to sulfate interacting with a tetragonal zirconia support.

We used *in situ* DRIFT to examine the state of the sulfate species under reaction conditions. The sulfated samples were heated under helium flow to 588 K for 1 h, the same pretreatment as used in *n*-butane isomerization. The temperature was then decreased to 553 K (reaction temperature) and a DRIFT scan taken. The effect of this treatment on the impregnated aerogel can be seen in Fig. 7. The primary difference seen upon heating was new fea-

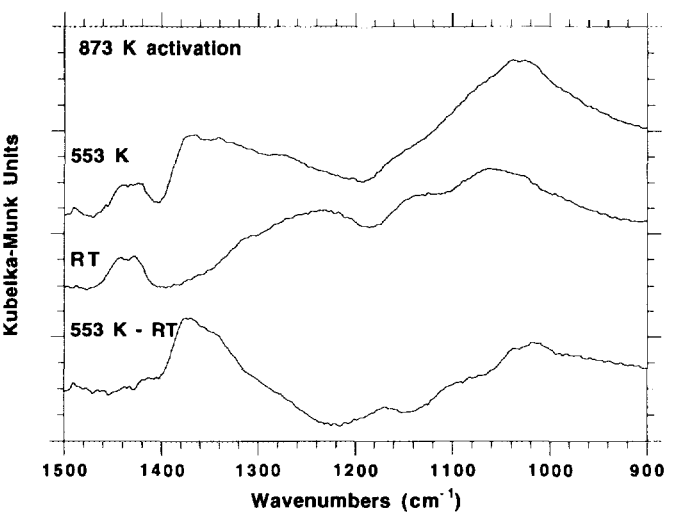

FIG. 7. In situ diffuse reflectance infrared spectra of A-Z/SO_4. Sample calcined at 873 K for 2 h. Top two spectra taken at indicated temperatures under He flow. The bottom spectra is the difference of the top two.

[3] In the text, when a support is termed active or inactive, the statement is referring to the ability of the support, after sulfate impregnation, to be active or inactive for *n*-butane isomerization.

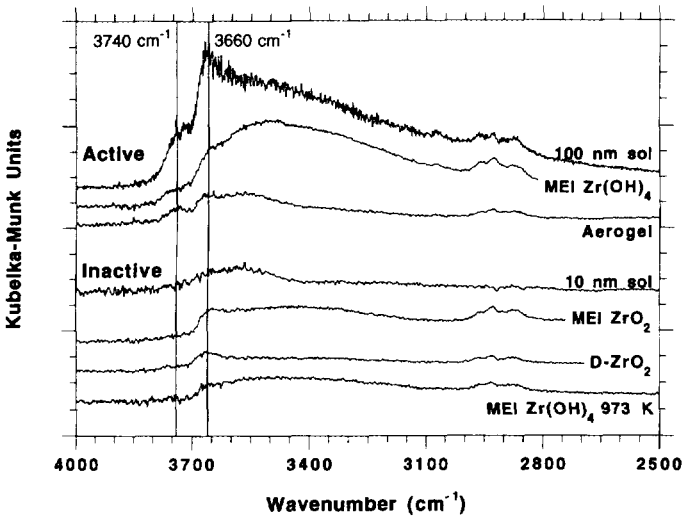

FIG. 8. *In situ* diffuse reflectance infrared spectra of zirconia supports. Samples were calcined at 773 K for 2 h unless another temperature is given. Spectra were taken at 673 K under vacuum.

tures in the 1300–1400 cm^{-1} range and these features were seen more clearly by subtracting the room-temperature scan from the high-temperature scan. Peak growth in this area corresponded to an increase in the covalent nature, or increased S=O bond order, of the sulfate ion (15, 16) as water was removed from the sample. In addition, we saw some changes in the lower wavenumber region. At the reaction temperature, we see that the primary DRIFT peak was at ca. 1020–1040 cm^{-1}. Similar experiments were run on all of the sulfated supports and also the zirconia sol–sulfate co-gels. In addition to some differences in relative peak intensities, all sulfated samples showed similar behavior under heating.

Hydroxyl content of supports. Since sulfate is added to the surface of these materials, the ability of the sulfate to anchor on the surface is perhaps related to the support hydroxyl content. We examined the nature of the surface hydroxyl groups on the zirconia supports by using *in situ* DRIFT. *Ex situ* DRIFT spectra were not helpful in distinguishing among supports due to the large amount of physisorbed water on most of the samples. This physisorbed water was removed by heating the sample to 673 K under a vacuum. Under these conditions, we were able to observe a difference between active and inactive supports (Fig. 8). Supports that were active for isomerization after sulfate impregnation exhibited two types of free (i.e., not participating in hydrogen bonding) –OH groups under DRIFT. Peaks at ca. 3740 and 3660 cm^{-1} which can be assigned to –OH groups bound to a solitary zirconium atom and to 2 or more zirconium atoms, respectively, were seen (17). On some samples, some hydrogen bonded –OH groups were still present as seen by the broad asymmetric peak with a maximum around 3500 cm^{-1}. Supports that were not active after impregnation exhibited only the type of free –OH group that is bonded to multiple zirconium atoms. For example, in Fig. 8, the top three spectra are for the 100 nm sol-derived material, aerogel, and MEI zirconium hydroxide. These three supports were active for *n*-butane isomerization after impregnation and exhibited the peak at 3740 cm^{-1}. The bottom four spectra in Fig. 8 were all from inactive supports and did not exhibit this peak. This is the most convincing difference seen between active and inactive supports.

DISCUSSION

Effect of Sulfate Introduction Point on Aerogel Properties

Texture. The texture of the sulfated aerogels varied greatly depending on the sulfate introduction point. The aerogel dried at 383 K had a significant surface-area and pore-volume loss after sulfate impregnation whereas the aerogel calcined at 773 K did not. The open porous structure of the aerogel can explain this phenomenon. When the alcogel was made by sol-gel chemistry, a polymeric network was formed. To retain this open polymeric network, the alcohol solvent was replaced by supercritical carbon dioxide (18). Since the supercritical CO_2 did not have a liquid–vapor interface, it could be removed from the gel without collapsing the pores as would occur during conventional evaporative drying. This supercritical drying yielded an aerogel with a porous structure. During the impregnation of the dried aerogel, water was placed into the pores of this material and then dried under vacuum. As the water evaporated, a liquid–vapor interface was allowed to form in the pores. This interface had a corresponding surface tension that caused the pores to collapse, resulting in the low surface area of A-Z-383/SO_4.

On the other hand, for the calcined aerogel, impregnation had only a small effect on the physical properties of the sample. The calcination of the support before impregnation formed a stronger oxide network with some pore collapse already having occurred. This resulting porous network was then able to withstand the capillary forces brought about by drying after impregnation and no further pore collapse took place.

Activation behavior. The response of the aerogel to activation temperature also varied with the sulfate introduction point and can be explained as follows. For the co-gel sample (10), sulfate was included in the gelation step. Thus, at low activation temperatures, sulfate was trapped in the bulk of the material where it could not modify the surface acidity and the sample was inactive (see Fig. 3).

When activated to higher temperatures, the support crystallized and expelled sulfate onto the surface of the material. Brønsted acidity was formed and isomerization activity was seen. Similar behavior was seen when sulfate was impregnated on the dried aerogel. Heat treatment after impregnation caused a great deal of sintering as mentioned above. Sulfate was trapped inside the sintered material, preventing surface modification, and an inactive material for isomerization was formed at low activation temperatures. As the activation temperature was increased, the material opened up forming micropores, increasing the surface area (Fig. 2) and allowing sulfate to modify the surface. This modified surface was then capable of *n*-butane isomerization. In addition, the low surface area of A-Z-383/SO_4 caused the density of sulfate on the surface to be large, possibly accounting for the high specific rate. One difference between this sample and the co-gel is that the expulsion of sulfate to the surface was not caused by crystallization. All of the A-Z-383/SO_4 samples examined (823 K activation and higher) were tetragonal. In this sample, the mechanism of sulfate expulsion was related to the opening up of the porous structure. The narrowness of the activation profile in Fig. 3 was due to the fact that the temperature required for this pore-opening mechanism was higher than the crystallization phenomenon for the co-gel. Thus, the temperature at which sulfate was expelled and an active sample was formed for A-Z-383/SO_4 was closer to the temperature at which surface decomposition began to occur, accounting for the narrow activation window for activity.

In contrast to the above two samples, the A-Z/SO_4 sample had a broad activation profile (Fig. 3). This sample was made by impregnating a calcined material. Since this structure did not collapse after impregnation, sulfate was on the surface of the material even at low activation temperatures. The only requirement of the activation step was to allow the sulfate to interact with the support. This sulfate–support interaction occurred at a lower temperature than the phenomena (crystallization for the co-gel and pore opening for A-Z-383/SO_4) described above. Thus, A-Z/SO_4 was active at a lower temperature and hence active over a broader range of temperatures. TG data support this conclusion. In Fig. 4, we see that A-Z-383/SO_4 demonstrated a Mode I-type peak caused by the loss of sulfate during expulsion from the bulk when the pores opened up with heat treatment. On the other hand, A-Z/SO_4, which contained all the sulfate on the surface, showed only Mode II weight loss due to surface sulfate decomposition.

The difference between having sulfate initially in the bulk and on the surface can also be seen in the sulfate region of the DRIFT spectra for the two impregnated aerogel samples (Fig. 5). The sulfate DRIFT region of A-Z-383/SO_4 changes with increasing heat treatment in a similar manner to the co-gel (10), consistent with sulfate trapped in the bulk at low temperatures and being expelled to the surface with more severe heat treatment. On the other hand, A-Z/SO_4 shows a relatively constant sulfate region, indicative of sulfate always being on the surface of the material.

The above data show that by changing the introduction point of sulfate, a material with different properties and activation behavior can be produced.

Importance of Zirconia Support Properties for Forming Active Samples

By a comparison of various calcined zirconia supports, we can elucidate the important support characteristics for the formation of active samples after sulfate impregnation. The crystal structure of the support was not a primary factor. Contrary to previous reports, we were able to impregnate both amorphous (A-ZrO_2 383 K) and crystalline supports to form samples that were active for *n*-butane isomerization. The structure of the crystalline support could be either tetragonal (the calcined aerogel and calcined MEI $Zr(OH)_4$) or monoclinic (100 ZrO_2 sol). While our previous work (10) demonstrated the importance of the tetragonal phase, the tetragonal phase alone did not create an active material as evidence by the 10-nm sol sample which was crystalline tetragonal and inactive. In addition, the 100-nm sol-derived sample was only weakly crystalline, primarily monoclinic, and active for isomerization after impregnation. However, it was an order of magnitude less active than the fully crystalline, primarily tetragonal samples. It was not clear whether this decreased activity was due to the monoclinic phase or its weakly crystalline nature.

Using DRIFT, we could not differentiate between active and inactive sulfate groups on these supports. The only observed difference was due to sulfate interacting with a tetragonal support. However, this was not a definitive sign of an active sulfate group as the sol-derived samples showed. The reason for the similarity among active and inactive samples was that the isomerization activity exhibited by these samples was probably created by only a small fraction of the sites on the samples. Many studies (7, 8, 15, 19, 20) determined that the number of sulfate groups or the Brønsted site density were not determining factors in the acidity. For example, Morterra *et al.* (19, 20) predicted that the superacidic sites, if Brønsted sites, were made up of only a few anhydrous protonic centers and that the catalytic activity of the sulfated zirconia was not sensitive to the overall amount of Brønsted acid sites. In another study (8), two samples with identical sulfate contents had different activities depending on whether the support was amorphous or crystalline. Thus, the DRIFT spectra of active and inactive samples looked alike because the important differences were made up by only a small

number of sites. In our previous work (10), we were able to detect differences using DRIFT between active and inactive samples. However, in that case we were looking at phenomena due to activation and sulfate content. In this study, all of the sulfate in our active samples may have underwent the described activation changes, but still only a small fraction of them actually participated in the generation of isomerization activity.

Figure 8 shows that the hydroxyl content of the zirconia supports was the critical factor in determining whether a support could generate an active sample with sulfate. The supports were partially dehydroxylated by heating to 673 K under vacuum. While this was not the state of the support during impregnation, it could be used as a fingerprint or indicator of the hydroxyl inventory during impregnation conditions. The three active supports (A-ZrO_2, MEI $Zr(OH)_4$, and the 100 nm ZrO_2 sol) all had free hydroxyls bound to both one zirconium atom (Type I hydroxyl) and two or more zirconium atoms (Type II hydroxyl). The inactive samples did not contain Type I hydroxyls at the elevated temperature.

The presence or absence of Type I hydroxyls can be related to the overall hydroxyl content. On a surface with only a small number of hydroxyl groups, bridging hydroxyls form that coordinate with two or more zirconium atoms. This allows for more zirconium atoms to reach their desired coordination number. A representative surface schematic of an inactive support, similar in structure to a zirconia surface proposed by Clearfield *et al.* (2), is shown in Fig. 9a. Only Type II hydroxyls are present and are represented by an –OH group bonded to two zirconium atoms (21, 22). These –OH groups are coming out of the plane of the zirconium atoms, or out of the plane of the page. In the tetragonal phase, the zirconium atoms are eight-fold coordinated. The other four bonds to each zirconium atom are Zr–O–Zr bonds beneath the –OH bridges below the Zr plane. It must be noted that different exposed crystal faces will have different ratios of external Zr–OH–Zr bridges to internal Zr–O–Zr bonds per zirconium atom. A surface similar to this one will contain only bridging –OH groups under partially dehydroxylated conditions.

As the hydroxyl content of the material increases, Type I hydroxyls bound to only a single zirconium atom will form to create room for the increased number of hydroxyl groups. This type of active support surface is shown in Fig. 9b. Here, both Type I and Type II hydroxyls are present coming out from the surface. As the hydroxyl content increases, the amount of Type I hydroxyls relative to Type II hydroxyls also increases. These highly hydroxylated surfaces will contain both Type I and Type II hydroxyls under partially hydroxylated conditions. Hence, we see that the presence of Type I hydroxyls can be correlated with the overall hydroxyl content.

The different preparation methods used can account for the differences in hydroxyl content of these samples. In the sol-gel synthesis, two reactions took place:

Hydrolysis

$$M(OR)_n + x\,H_2O \rightarrow M(OR)_{n-x}(OH)_x + x\,ROH \quad [1]$$

Condensation

$$M\text{-}OH + HO\text{-}M \rightarrow M\text{-}O\text{-}M + H_2O \quad [2a]$$

$$M\text{-}OR + HO\text{-}M \rightarrow M\text{-}O\text{-}M + ROH. \quad [2b]$$

The final gel had many terminal –OH and –OR groups in the structure that, after drying and calcination, yielded a high hydroxyl content on the surface of the aerogel. This high hydroxyl content translated into a high content of Type I hydroxyls, some of which still remained at the elevated temperature used to take the spectra in Fig. 8. While the exact preparation method is unknown to us, the MEI zirconium hydroxide was most likely made by some sort of low-temperature precipitation method that also yielded a high hydroxyl content. On the other hand, the MEI and Degussa ZrO_2 samples were made by high-temperature routes. MEI calcines a chemically precipitated intermediate (23) while Degussa uses the flame hydrolysis of $ZrCl_4$ (24). These higher temperature synthetic methods apparently yielded materials with a very low hydroxyl content and hence predominantly Type II hydroxyls. The MEI zirconium hydroxide after 773 K calcination had a large hydroxyl content and Type I hydroxyls as seen in Fig. 8. However, increased heat treatment to 973 K further dehydroxylated the support decreasing the hydroxyl inventory and eliminating Type I hydroxyls. The sol samples were shown in our previous work (13) to have a hydroxyl inventory dependent on sol size such that the 10 nm sol had a smaller hydroxyl inventory than the 100 nm sol.

While most previous reports stated that it was the crystallinity of the support that determined strong acidity, we believe that it was, in fact, the hydroxyl content of the support. If a synthesis method yielded the appropriate type and number of hydroxyls on the surface, the crystallinity was of lesser importance. We believe that it was the Type I hydroxyls, in conjunction with a large overall hydroxyl content, that acted as anchoring sites for sulfate to form samples that are active in isomerizing *n*-butane. Sulfate also anchored on Type II hydroxyls as seen by the fact that samples with a low or nonexistent population of Type I hydroxyls did contain sulfate after impregnation. However, these sulfate ions did not create isomerization activity. There is evidence that the Type I hydroxyl site is preferential for adsorption. CO_2 adsorption on a pure zirconia support showed that hydrogenocarbonates formed at Type I hydroxyls but not Type II (25). When a zirconia support was sulfated by SO_2 oxidation, the IR peak for Type I

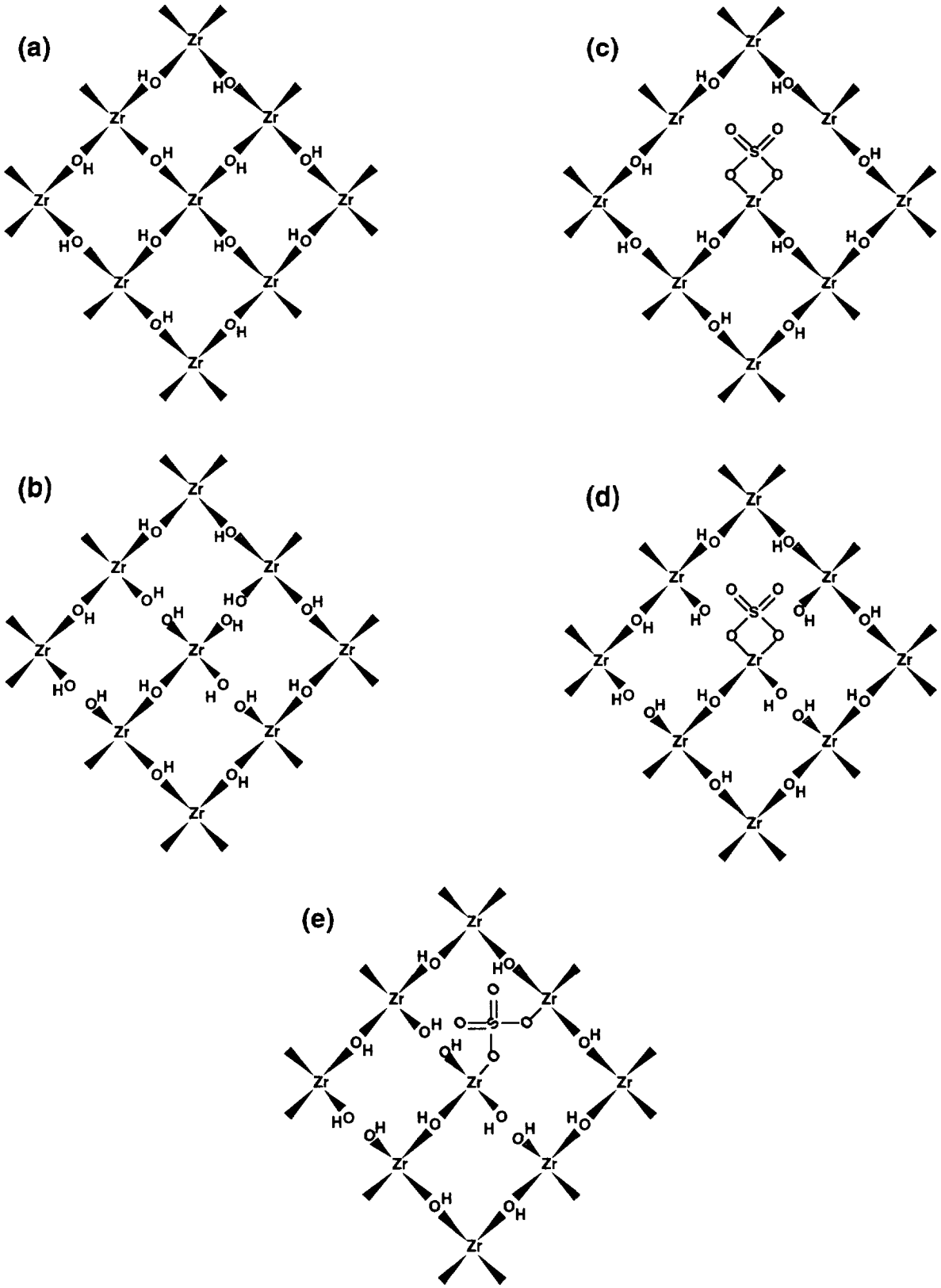

FIG. 9. Schematic representations of the surfaces of zirconia supports and sulfated zirconias. (a) An inactive support dominated by Type II hydroxyls. (b) An active support containing both Type I and Type II hydroxyls. (c) A sulfate group interacts with an inactive support to form a bidentate chelating sulfate. (d) A sulfate group interacts with an active support to form a bidentate chelating sulfate. (e) A sulfate group interacts with an active support to form a bidentate bridging sulfate.

hydroxyls disappeared while the Type II peak remained (26). Impregnation of a zirconium hydroxide by sulfuric acid immersion also resulted in a significant decrease of Type I hydroxyls (21). Because of this decrease in Type I hydroxyl content after sulfate impregnation, the –OH signature of a support must be examined before impregnation in order to determine its ability to form an active sample. If an active support is examined after impregnation, it might appear to be an inactive support because the Type I hydroxyls were consumed by sulfate anchoring.

The interactions between the sulfate groups and Type I and Type II hydroxyls will determine what kind of sulfate species is formed on the zirconia surface and how it becomes active. Jin *et al.* (15, 16) proposed a chelating bidentate sulfate structure. Given the location of an *ex situ* DRIFT peak in the 1220–1270 cm^{-1} region (Fig. 5), our data also indicated the presence of these chelating sulfates (27) under hydrated conditions. The additional presence of bridging sulfate groups on our samples could not be ruled out. Lavalley and co-workers (28, 29) proposed a sulfate structure that under dehydrated conditions contained only a single S=O bond and a sulfur atom which was bonded to the support by three Zr–O–S bonds. They also postulated the existence of an $S_2O_7^{2-}$ species under high sulfate loading. Their IR spectra were very similar to ours and to those of Jin *et al.* (15, 16) but Lavalley and co-workers made their different assignment on the basis of oxygen-18 exchange (30). As mentioned in our previous work (10), the differences between these two models, in terms of the number of S=O double bonds and Zr–O–S bonds, are not critically important because both of these models share an important characteristic: the presence of the S=O double bond that can act as an electron inductor. In the model of Lavalley and co-workers (28, 29), the requirement of three Zr–O–S bonds simply increases the importance of a highly hydroxylated surface to guarantee three zirconium atoms with the appropriate hydroxyl groups for sulfate anchoring.

Most recent studies found both Brønsted and Lewis acidity on the surface of sulfated zirconia (1, 2, 7, 9, 19–21, 31, 32). While the exact role of these two types of acidity in the isomerization mechanism is not completely known, the required presence of Brønsted acidity for the reaction has been shown in our work (10) and others (1, 7, 28). The location of the Brønsted proton and how the sulfate interacts with the surface to form this Brønsted acidity is in debate. Some reports (2, 9, 19, 21) stated that the proton was in the coordination sphere of the sulfate group. This seems unlikely for a number of reasons. First, most models for such a bisulfate species were derived using sulfuric acid as the sulfate source. However, other sulfate impregnation methods (15, 28, 33), such as ammonium sulfate impregnation or SO_2 oxidation, yielded materials with properties similar to the sulfuric acid-promoted materials. In these alternate preparations, the formation of a bisulfate species on the surface is not as plausible. In addition, in our work (10) and in others (19, 20, 28), the state of the sulfate species was seen to change upon heating and dehydration. This was thought to be due to the removal of water which allowed the sulfate ion to transform from an ionic type of species with a reduced S=O bond order, such as a bisulfate species, to a more covalent species, such as SO_4^{2-} without a proton. Since it was this covalent species that was present under reaction conditions as shown by *in situ* DRIFT, it was unlikely that a bisulfate group was responsible for the acidic proton.

Another model suggests that water converts a Lewis site to a Brønsted site as follows (4):

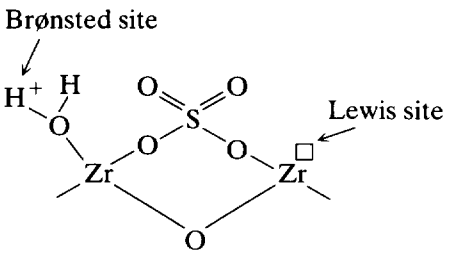

However, recent reports stating that water was a poison and not a promoter (8, 19, 34) would seem to discount this model.

We believe that the acidic proton was derived from a hydroxyl group on the zirconia support near a covalent sulfate group with S=O double bonds. Sulfate interacts with surfaces of different hydroxyl contents in different ways. On the inactive surface (Fig. 9a), sulfate will interact with a single zirconium atom, displacing two of the bridging –OH groups (Type II hydroxyls) forming a bidentate chelating sulfate species (Fig. 9c). The charge in solution is balanced by the formation of two OH^- anions from the displaced bridged –OH groups to replace the doubly charged SO_4^{2-} removed from solution. To satisfy their desire for eight-fold coordination, the other zirconium atoms involved in the removed –OH bridges potentially coordinate with the oxygen atoms of the Zr–O–S bonds. While it would be possible for the sulfate group to form a bridging species by replacing a single –OH bridge (another –OH-bridge would have to be removed for charge balance), this formation seems less desirable as it would not have the added benefit of the above-mentioned coordination expansion between undercoordinated Zr and the Zr–O–S oxygen atom. On the active surface (Fig. 9b), sulfate can interact with the surface in a number of different ways. It can displace two Type I hydroxyls to form either a chelating (Fig. 9d) or bridging (Fig. 9e) bidentate sulfate. It could also displace one Type I and one Type II hydroxyl to form again either a bridging or chelating sulfate. Finally, two

Type II hydroxyls could be displaced forming a chelating sulfate as on the inactive support (Fig. 9c).

The sulfate species that generated strong acidity was one that interacted with a surface containing Type I hydroxyls. We have two reasons for this proposal: the strength of the anchoring Zr–O–S bonds and the overall hydroxyl content. In the case of inactive supports, the hydroxyls were all Type II bridged –OH groups. Here, the electronic charge which made up the Zr–OH–Zr bridge was delocalized and split between the two Zr–OH bonds. On an active support, Type I –OH groups had very localized Zr–OH bonds because the electronic charge between the Zr and O atoms were not shared with another bond. Thus, when sulfate displaced a Type I hydroxyl, the resulting Zr–O–S bond was localized and hence stronger than a delocalized one, whereas the Type II –OH site yielded a weaker Zr–O–S bond due to a lower available electron density. We speculate that the strength or electronic density in the area of this bond dictated how strong the electron induction effect of the sulfate double bonds could be. A strong Zr–O–S bond allowed for easy charge transfer away from a neighboring surface –OH toward the S=O bonds. If the Zr–O–S bond was not strong, this charge transfer was hampered. It was this charge transfer that created a Brønsted acid site from a neighboring –OH group. Thus, Type I –OH groups were required to form a strong Zr–O–S bond capable of forming an acidic site.

Once the appropriate sulfate group was formed on the surface, a Zr–OH group must be sufficiently close to generate a Brønsted acid site by the electron induction effect of the sulfate group. As mentioned above, active supports with Type I hydroxyls were more highly hydroxylated than inactive supports. This higher hydroxylation yielded a higher probability that the ziconium atom to which a given sulfate was attached also had another hydroxyl group in its coordination sphere, or sufficiently close by, capable of forming acidity. Afanasiev *et al.* (35) proposed such a model where the metal cation must be coordinated with one or more promoter (molybdate, tungstate, of sulfate) groups and also a hydroxyl group that provides the proton for Brønsted acidity.

Supports with Type I hydroxyls were active for *n*-butane isomerization regardless of the support crystal structure. However, when the 100-nm sol support was compared with other active supports, the sulfated 100-nm sol-derived support was less active. As mentioned above, the cause for this decreased activity was due to either the monoclinic phase, the weakly crystalline nature of the 100 Zr support, or both. A crystalline support was preferential for helping to promote the charge transfer (36) between neighboring –OH and sulfate groups that created acidity as mentioned above. An amorphous or weakly crystalline support could weaken this charge transfer. In addition, since each zirconium atom in the monoclinic phase, with a reduced coordination number of 7, was coordinated to fewer oxygens or hydroxyls, the probability that a zirconium atom was coordinated to enough hydroxyl groups for both sulfate modification and acidity generation also decreased. These possibilities combined to describe how the monoclinic phase could be less desirable than the tetragonal phase as a support. Again, though, it must be noted that a weakly monoclinic structure can form an active sample upon sulfate impregnation given the appropriate hydroxyl content on the surface.

CONCLUSIONS

The sol-gel preparation of zirconium oxide formed supports with properties not found in other synthetic methods and these differences allowed us to determine the properties required of a support to form *n*-butane isomerization activity upon sulfate impregnation. First, the point of sulfate introduction in the zirconia aerogel synthesis had important consequences on the texture and activation behavior of sulfated zirconia. In this paper, we saw the differences caused by impregnating the aerogel after vacuum drying and after calcination. The first method caused a large amount of pore collapse, trapping sulfate in the bulk of the low-surface-area material. Subsequent heat treatment caused the pores of the material to open up, which allowed sulfate to modify the surface of the material and to generate *n*-butane isomerization activity. When sulfate was placed on a calcined zirconia aerogel, no textural change was noted after impregnation and the activation window for activity was much wider due to sulfate being initially present on the surface.

This calcined, crystalline zirconia aerogel was active for *n*-butane isomerization after sulfate impregnation, in contrast with the vast majority of literature reports. Because of this finding, we were able to compare this active support with other active and inactive calcined supports to determine what properties were necessary for generating acidity. The most important factor in determining a desirable support was the hydroxyl content of the surface. A high hydroxyl content, characterized by the presence of free hydroxyl groups bound to a single zirconium atom, was required for the support to be active for *n*-butane isomerization after sulfate impregnation. This high hydroxyl content yielded sulfate groups with strong Zr–O–S bonds which combined with adjacent surface Zr–OH groups to create strong Brønsted acidity by the electron induction effect of the S=O double bonds. Synthetic methods that can deliver this high hydroxyl content can form active supports. Other factors, such as the crystal structure of the support, play secondary roles in determining the degree of acidic activity observed.

ACKNOWLEDGMENTS

This work was supported by the National Science Foundation (CTS-9200665). D.A.W. thanks the Texaco Foundation for the support of a graduate fellowship. We also thank Degussa, Magnesium Elektron (MEI), and Nyacol Products for providing us with samples.

REFERENCES

1. Davis, B. H., Keogh, R. A., and Srinivasan, R., *Catal. Today* **20,** 219 (1994).
2. Clearfield, A., Serrette, G. P. D., and Khazi-Syed, A. H., *Catal. Today* **20,** 295 (1994).
3. Tanabe, K., Hattori, H., and Yamaguchi, T., *Crit. Rev. Surf. Chem.* **1,** 1 (1990).
4. Arata, K., *in* "Advances in Catalysis" (D. D. Eley, H. Pines, and P. B. Weisz, Eds.), Vol. 37, p. 165, Academic Press, San Diego, 1990.
5. Hino, M., Kobayashi, S., and Arata, K., *J. Am. Chem. Soc.* **101,** 6439 (1979).
6. Morterra, C., Cerrato, G., Emanuel, C., and Bolis, V., *J. Catal.* **142,** 349 (1993).
7. Chen, F. R., Coudurier, G., Joly, J.-F., and Vedrine, J. C., *J. Catal.* **143,** 616 (1993).
8. Comelli, R. A., Vera, C. R., and Parera, J. M., *J. Catal.* **151,** 96 (1995).
9. Riemer, T., Spielbauer, D., Hunger, M., Mekhemer, G. A. H., Knözinger, H., *J. Chem. Soc., Chem. Commun.*, 1181 (1994).
10. Ward, D. A., and Ko, E. I., *J. Catal.* **150,** 18 (1994).
11. Ward, D. A., and Ko, E. I., *Chem. Mater.* **5,** 956 (1993).
12. Cheng, C.-P., Iacobucci, P. A., and Walsh, E. N., U.S. Patent 4,619,908, Oct. 28, 1986.
13. Ward, D. A., and Ko, E. I., *Langmuir* **11,** 369 (1995).
14. Toraya, H., Yoshimura, M., and Sōmiya, S., *J. Am. Ceram. Soc.* **67,** C-119 (1984).
15. Jin, T., Yamaguchi, T., and Tanabe, K., *J. Phys. Chem.* **90,** 4794 (1986).
16. Yamaguchi, T., Jin, T., and Tanabe, K., *J. Phys. Chem.* **90,** 3148 (1986).
17. Agron, P. A., Fuller, E. L., and Holmes, H. F., *J. Colloid Interface Sci.* **52,** 553 (1975).
18. Ayen, R. J., and Iacobucci, P. A. *Rev. Chem. Eng.* **5,** 157 (1988).
19. Morterra, C., Cerrato, G., Pinna, F., Signoretto, M., and Strukul, G., *J. Catal.* **149,** 181 (1994).
20. Morterra, C., Cerrato, G., Pinna, F., and Signoretto, M., *J. Phys. Chem.* **98,** 12373 (1994).
21. Kustov, L. M., Kazansky, V. B., Figueras, F., and Tichit, D., *J. Catal.* **150,** 143 (1994).
22. Tsyganenko, A. A., and Filimonov, V. N., *J. Mol Struct.* **19,** 579 (1973).
23. Product Data Sheet Number 305A, Magnesium Electron, Inc.
24. Technical Bulletin Pigments No. 56, Degussa.
25. Bensitel, M., Moravek, V., Lamotte, J., Saur, O., and Lavalley, J. C., *Spectrochim. Acta Part A* **43,** 1487 (1987).
26. Bensitel, M., Saur, O., Lavelley, J. C., and Mabilon, G., *Mater. Chem. Phys.* **17,** 249 (1987).
27. Nakamoto, K., "Infrared Spectra of Inorganic and Coordination Compounds." Wiley-Interscience, New York, 1970.
28. Bensitel, M., Saur, O., Lavalley, J.-C., and Morrow, B. A., *Mater. Chem. Phys.* **19,** 147 (1988).
29. Waqif, M., Bachelier, J., Saur, O., and Lavalley, J.-C., *J. Mol. Catal.* **72,** 127 (1992).
30. Saur, O., Bensitel, M., Mohammed Saad, A. B., Lavalley, J. C., Tripp, C. P., and Morrow, B. A., *J. Catal.* **99,** 104 (1986).
31. Adeeva, V., de Haan, J. W., Janchen, J., Lei, G. D., Schunermann, V., van de Ven, L. J. M., Sachtler, W. M. H., and van Santen, R. A., *J. Catal.* **151,** 364 (1995).
32. Lunsford, J. H., Sang, H., Campbell, S. M., Liang, C.-H., and Anthony, R. G., *Catal. Lett.* **27,** 305 (1994).
33. Sohn, J. R., and Kim, H. W., *J. Mol. Catal.* **52,** 361 (1989).
34. Keogh, R. A., Srinivasan, R., and Davis, B. H., *J. Catal.* **151,** 292 (1995).
35. Afanasiev, P., Geantet, C., Breysse, M., Coudurier, G., and Vedrine, J. C., *J. Chem. Soc. Faraday Trans.* **90,** 193 (1994).
36. Ishida, T., Yamaguchi, T., and Tanabe, K., *Chem. Lett.*, 1869 (1988).